# Suppression of the Jahn-Teller Distortion in a Six-Coordinate Copper(II) Complex by Doping it into a Host Lattice

Rebecca Docherty, Floriana Tuna, Colin A. Kilner, Eric J. L. McInnes*
and Malcolm A. Halcrow*

## Supporting Information

**Experimental procedures**

**Table S1** Elemental microanalyses of the materials in this work.

**Table S2** Experimental details for the crystal structure determinations in this work.

**Figure S1** View of the complex dication in $[Cu(terpy)_2][BF_4]_2$ at 150 K.

**Table S3** Selected bond lengths and angle**s** in the crystal structures of $[Cu(terpy)_2][BF_4]_2$.

**Figure S2** Observed and simulated *X*-band EPR spectra of $[Cu(terpy)_2][BF_4]_2$ as a pure powder.

**Figure S3** *X*-ray powder diffraction data for the precursor compounds $[M(bpp)_2][BF_4]_2$ and $[M(terpy)_2][BF_4]_2$ ($M^{2+}$ = $Fe^{2+}$, $Cu^{2+}$ and $Zn^{2+}$).

**Table S4** Spin-crossover parameters for **1a** and **2a**, from magnetic susceptibility and DSC measurements.

**Figure S4** Magnetic susceptibiliy data for **1a** and **2a**.

**Figure S5** Comparison of the *X*-ray powder diffraction patterns of **1a** and **1b** with those of the undoped host lattices $[M(bpp)_2][BF_4]_2$ ($M^{2+}$ = $Fe^{2+}$ or $Zn^{2+}$).

**Figure S6** *X*-band EPR spectra of **1a**.

**Figure S7** Experimental and simulated *X*-band EPR spectra of **1b**.

**Figure S8** Comparison of the *X*-ray powder diffraction patterns of **2a** and **2b** with those of the undoped host lattices $[M(bpp)_2][BF_4]_2$ ($M^{2+}$ = $Fe^{2+}$ or $Zn^{2+}$).

**Figure S9** *X*-band EPR spectra of **2a**.

**Figure S10** *X*-band EPR spectra of **2b**.

**Figure S11** Experimental and simulated *Q*-band EPR spectra of **2a**.

**Figure S12** Experimental and simulated *X*-band EPR spectrum of **2b**.

**Figure S13** Comparison of the *X*-ray powder diffraction patterns of **3a** and **3b** with those of the undoped host lattices $[M(terpy)_2][BF_4]_2$ ($M^{2+}$ = $Fe^{2+}$ or $Zn^{2+}$).

**Figure S14** *X*-band EPR spectra of **3a**.

**Figure S15** *X*-band EPR spectra of **3b**.

**Figure S16** *Q*-band EPR spectra of **3a**.

**Experimental procedures**

The precursor complexes $[M(bpp)_2][BF_4]_2$ (M = Fe,[1] Cu,[2] Zn[3]) were prepared by the literature procedures. The salts $[M(terpy)_2][BF_4]_2$ (M = Fe, Cu and Zn) were prepared by stirring $Fe[BF_4]_2 \cdot 6H_2O$ (0.18 g, 0.54 mmol), $Cu[BF_4]_2 \cdot 4H_2O$ (0.17 g, 0.54 mmol) or $Zn[BF_4]_2 \cdot 6H_2O$ (0.19 g, 0.54 mmol) with terpy (0.25 g, 1.07 mmol) in $MeNO_2$ (25 $cm^3$) at room temperature until all the solid had dissolved. Concentration of the solution and crystallization with diethyl ether yielded dark purple (M = Fe), blue-green (M = Cu) or pale pink (M = Zn) prisms. The dried iron complex analysed consistently as its hemihydrate, while the copper and zinc complexes were solvent-free.

Characterisation data for $[Fe(terpy)_2][BF_4]_2 \cdot \frac{1}{2}H_2O$: found  C, 50.8; H, 3.05; N, 11.9 %. Calcd for $C_{30}H_{22}B_2F_8FeN_6 \cdot \frac{1}{2}H_2O$ C, 51.1; H, 3.29; N, 11.9 %. ES mass spectrum: $m/z$ 234.1 (8 %, $[H(terpy)]^+$), 261.1 (100 %, $[Fe(terpy)_2]^{2+}$), 541.1 (7 %, $[Fe(terpy)_2F]^+$), 609.1 (4 %, $[Fe(terpy)_2(BF_4)]^+$).

Characterisation data for $[Cu(terpy)_2][BF_4]_2$: found  C, 51.0; H, 3.10; N, 11.8 %. Calcd for $C_{30}H_{22}B_2CuF_8N_6$ C, 51.2; H, 3.15; N, 11.9 %. ES mass spectrum: $m/z$ 234.1 (100 %, $[H(terpy)]^+$), 264.6 (77 %, $[Cu(terpy)_2]^{2+}$), 296.0 (8 %, $[Cu_2(terpy)_2]^{2+}$), 529.1 (8 %, $[Cu(terpy)_2]^+$).

Characterisation data for $[Zn(terpy)_2][BF_4]_2$: found  C, 50.8; H, 3.05; N, 11.7 %. Calcd for $C_{30}H_{22}B_2F_8N_6Zn$ C, 51.1; H, 3.14; N, 11.9 %. ES mass spectrum: $m/z$ 234.1 (59 %, $[H(terpy)]^+$), 265.1 (100 %, $[Zn(terpy)_2]^{2+}$), 549.1 (8 %, $[Zn(terpy)_2F]^+$), 617.1 (6 %, $[Zn(terpy)_2(BF_4)]^+$).

The solid solutions were prepared by recrystallizing solutions of the copper dopant (0.015 mmol) and the relevant host compound (0.35 mmol) in $MeNO_2$ (5 $cm^3$), by slow diffusion of diethyl ether vapor. The resultant polycrystalline materials were manually ground to a powder for analysis. Elemental microanalysis data for the solid solutions are given in Table S1.

CHN microanalyses were performed by the University of Leeds School of Chemistry microanalytical service, while metal analyses were carried out by the microanalytical service at the University of Manchester. Electrospray mass spectra were obtained using a Waters Micromass LCT TOF spectrometer, from MeCN solution. Powder diffraction data were obtained with a Bruker D8 diffractometer using Cu-$K_\alpha$ radiation ($\lambda$ = 1.5418 Å). DSC measurements employed a TA Instruments DSC 2010 scanning calorimeter, with a temperature ramp of 5 K $min^{-1}$. Variable temperature magnetic susceptibility measurements were obtained using a Quantum Design SQUID magnetometer. Diamagnetic corrections for the sample (from Pascal's constants[4]) and the sample holder were applied to the data.

$X$-band and $Q$-band EPR spectra were run using Bruker EMX spectrometers. These spectra were simulated using Bruker *SimFonia*, and *EasySpin*.[5]

**Single crystal structure determinations**

Single crystals of $[Cu(terpy)_2][BF_4]_2$ were grown by slow diffusion of diethyl ether vapor into a solution of the complex in nitromethane. Diffraction data were acquired using a Bruker X8 Apex II diffractometer fitted with an Oxford Cryostream low temperature device, using graphite-monochromated Mo-$K_\alpha$ radiation ($\lambda = 0.71073$ Å) generated by a rotating anode. The structures were solved by direct methods (*SHELXS97*[6]), and developed by cycles of full least-squares refinement on $F^2$ and difference Fourier syntheses (*SHELXL97*[6]). All crystallographic Figures were produced using *XSEED*,[7] which incorporates *POVRAY*.[8] The MSDA calculations in Table S3 were performed using P*LATON*.[9] Experimental data for the crystal structures are listed in Table S2, and bond lengths and angles from the structures are in Table S3.

The same crystal (a racemic twin) was used for data collections at 150 and 300 K. Both $BF_4^-$ ions are disordered at 300 K, one over two equally occupied sites sharing a common wholly occupied B atom; and, the other over three equally occupied orientations, two of which shared the same B atom which therefore had occupancy 0.67. The refined restraints B–F = 1.39(2) and F...F = 2.27(2) Å were applied to these groups. At 150 K, only the latter anion was still disordered, now over two sites with refined occupancies of 0.57:0.43. The same restraints were applied, which refined to B–F = 1.40(2) and F...F = 2.29(2) Å at this temperature. In both refinements, all wholly occupied non-H atoms were refined anisotropically, while H atoms were placed in calculated positions and refined using a riding model. Both structures have two residual Fourier peaks of $\leq 2.4$ $e$.Å$^{-3}$ in the vicinity of the Cu atom.

CCDC 866481 and 866482.

**Table S1** Elemental microanalyses of the solid solution materials in this work. The estimated error on $y$, based on these data, is ±0.01.

| | $y$ | C | H | N | Fe or Zn | Cu |
|---|---|---|---|---|---|---|
| $[Cu(terpy)_2]_y[Fe(bpp)_2]_{1-y}[BF_4]_2$ (**1a**) | 0.04 | 41.0 (41.0) | 2.75 (2.80) | 21.2 (21.1) | 8.2 (8.1) | 0.3 (0.4) |
| $[Cu(terpy)_2]_y[Zn(bpp)_2]_{1-y}[BF_4]_2$ (**1b**) | 0.04 | 40.4 (40.5) | 2.70 (2.76) | 20.8 (20.8) | 9.4 (9.5) | 0.3 (0.4) |
| $[Cu_yFe_{1-y}(bpp)_2][BF_4]_2$ (**2a**) | 0.03 | 40.6 (40.5) | 2.70 (2.78) | 21.6 (21.5) | 8.4 (8.3) | 0.2 (0.3) |
| $[Cu_yZn_{1-y}(bpp)_2][BF_4]_2$ (**2b**) | 0.03 | 40.1 (40.0) | 2.65 (2.74) | 21.2 (21.2) | 9.5 (9.6) | 0.3 (0.3) |
| $[Cu(bpp)_2]_y[Fe(terpy)_2]_{1-y}[BF_4]_2 \cdot \frac{1}{2}H_2O$ (**3a**) | 0.03 | 50.5 (50.8) | 3.10 (3.28) | 12.0 (12.2) | 7.9 (7.7) | 0.2 (0.3) |
| $[Cu(bpp)_2]_y[Zn(terpy)_2]_{1-y}[BF_4]_2$ (**3b**) | 0.02 | 50.6 (50.7) | 3.05 (3.13) | 12.1 (12.1) | 9.0 (9.1) | 0.1 (0.2) |

**Table S2** Experimental details for the crystal structure determinations of [Cu(terpy)$_2$][BF$_4$]$_2$
(C$_{30}$H$_{22}$B$_2$CuF$_8$N$_6$, fw 703.70).

| $T$ (K) | 300(2) | 150(2) |
|---|---|---|
| crystal syst | Monoclinic | Monoclinic |
| space group | *Cc* | *Cc* |
| $a$ (Å) | 12.7056(10) | 12.6690(10) |
| $b$ (Å) | 12.6356(11) | 12.5211(10) |
| $c$ (Å) | 19.7176(17) | 19.4354(16) |
| $\beta$ (°) | 95.378(4) | 95.776(4) |
| $V$ (Å$^3$) | 3151.6(5) | 3067.4(4) |
| $Z$ | 4 | 4 |
| $D_c$ (Mg.m$^{-3}$) | 1.483 | 1.524 |
| $F(000)$ | 1420 | 1420 |
| $\lambda$ (nm) | 0.71073 | 0.71073 |
| $\mu$(Mo-K$_\alpha$) (mm$^{-1}$) | 0.772 | 0.793 |
| total data collected | 23962 | 33789 |
| independent reflections | 6565 | 7025 |
| $R_{int}$ | 0.057 | 0.069 |
| $R_1$, w$R_2$ [$I > 2\sigma(I)$] | 0.072, 0.196 | 0.071, 0.197 |
| $R_1$, w$R_2$ [all data] | 0.085, 0.206 | 0.077, 0.204 |
| Flack parameter | 0.29(2) | 0.207(18) |
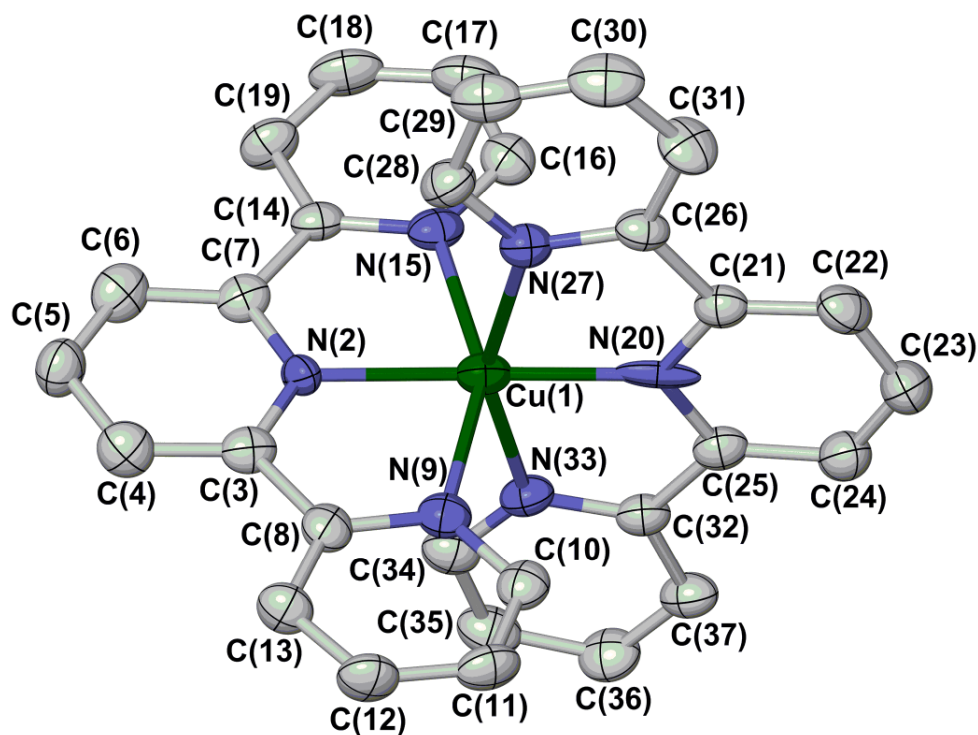


**Figure S1** View of the complex dication in [Cu(terpy)$_2$][BF$_4$]$_2$ at 150 K, showing the atom
numbering scheme employed. Atomic displacement parameters are at the 50 % probability
level, and H atoms have been omitted for clarity. Color code: C, white; Cu, green; N, blue.

**Table S3** Selected bond lengths and angles in the crystal structures of [Cu(terpy)$_2$][BF$_4$]$_2$ (Å, °). See Fig. S1 for the atom numbering scheme employed. The values in square brackets are $\langle d^2 \rangle$ ($10^4$ Å$^2$), calculated from the mean square displacement amplitudes (MSDAs) of the relevant Cu and N donor atoms.

| $T$ (K) | 300 | 150 |
|---|---|---|
| Cu(1)–N(2) | 2.061(5) [386(27)] | 2.079(4) [212(22)] |
| Cu(1)–N(9) | 2.225(6) [34(27)] | 2.206(5) [61(20)] |
| Cu(1)–N(15) | 2.232(6) [47(27)] | 2.237(5) [37(19)] |
| Cu(1)–N(20) | 1.971(9) [616(40)] | 1.976(8) [616(29)] |
| Cu(1)–N(27) | 2.207(5) [44(30)] | 2.205(4) [26(20)] |
| Cu(1)–N(33) | 2.224(5) [38(30)] | 2.228(4) [39(20)] |
| | | |
| N(2)–Cu(1)–N(9) | 77.8(2) | 77.04(18) |
| N(2)–Cu(1)–N(15) | 76.7(2) | 77.04(19) |
| N(2)–Cu(1)–N(20) | 178.9(2) | 178.0(3) |
| N(2)–Cu(1)–N(27) | 104.2(2) | 101.86(16) |
| N(2)–Cu(1)–N(33) | 102.1(2) | 103.54(16) |
| N(9)–Cu(1)–N(15) | 154.4(2) | 154.07(17) |
| N(9)–Cu(1)–N(20) | 102.4(2) | 101.19(19) |
| N(9)–Cu(1)–N(27) | 93.77(19) | 93.18(16) |
| N(9)–Cu(1)–N(33) | 93.77(19) | 94.60(16) |
| N(15)–Cu(1)–N(20) | 103.2(2) | 104.71(19) |
| N(15)–Cu(1)–N(27) | 91.89(19) | 91.13(16) |
| N(15)–Cu(1)–N(33) | 92.1(2) | 92.39(16) |
| N(20)–Cu(1)–N(27) | 76.9(2) | 77.26(17) |
| N(20)–Cu(1)–N(33) | 76.8(2) | 77.42(17) |
| N(27)–Cu(1)–N(33) | 153.6(2) | 154.50(16) |

An axis of pseudo-Jahn-Teller elongation would normally be observed along either of the directions N(9)−Cu(1)−N(15) or N(27)−Cu(1)−N(33), but this is not apparent at either temperature. Hence, this elongation axis is probably disordered between these two directions in the crystal.[10,11]

The $\langle d^2 \rangle$ values are the difference between the mean-square displacement amplitudes (MSDAs) for each Cu and donor N-atom (equations 1 and 2).[12]

$$MSDA = \left[ \sum_{i=1}^{3} \sum_{j=1}^{3} U_{ij} n_i n_j \right] / |n|^2 \qquad (1)$$

$$<d^2> = MSDA(N) - MSDA(Cu) \qquad (2)$$

where $U_{ij}$ is an element of the 3x3 matrix of thermal parameters and $n_i$, $n_j$ are elements of the vector **n** describing the bond. Although the errors are high and this parameter must be interpreted with care, Cu–N bonds showing $<d^2> > 100 \times 10^4$ Å$^2$ are often taken to indicate the presence of librational disorder in the metal coordination sphere, that is unresolved in the crystallographic refinement.[13] This is only a fingerprint that disorder of some type is present – it is not always possible to infer the form of this librational disorder from the $\langle d^2 \rangle$ values of the Cu–N bonds, taken in isolation.

The very high $\langle d^2 \rangle$ values shown by the bonds Cu(1)–N(2) and Cu(1)–N(20) strongly support the above suggestion, of unresolved pseudo-Jahn-Teller elongation in [Cu(terpy)$_2$][BF$_4$]$_2$. The fact that the Cu−N bond lengths and $\langle d^2 \rangle$ values are almost identical within experimental error at 300 and 150 K implies that this disorder may be static; or, if it is dynamic, it is only frozen out at much lower temperatures.

This conclusion is supported by the *X*-band EPR spectra of the compound (Fig. S2).
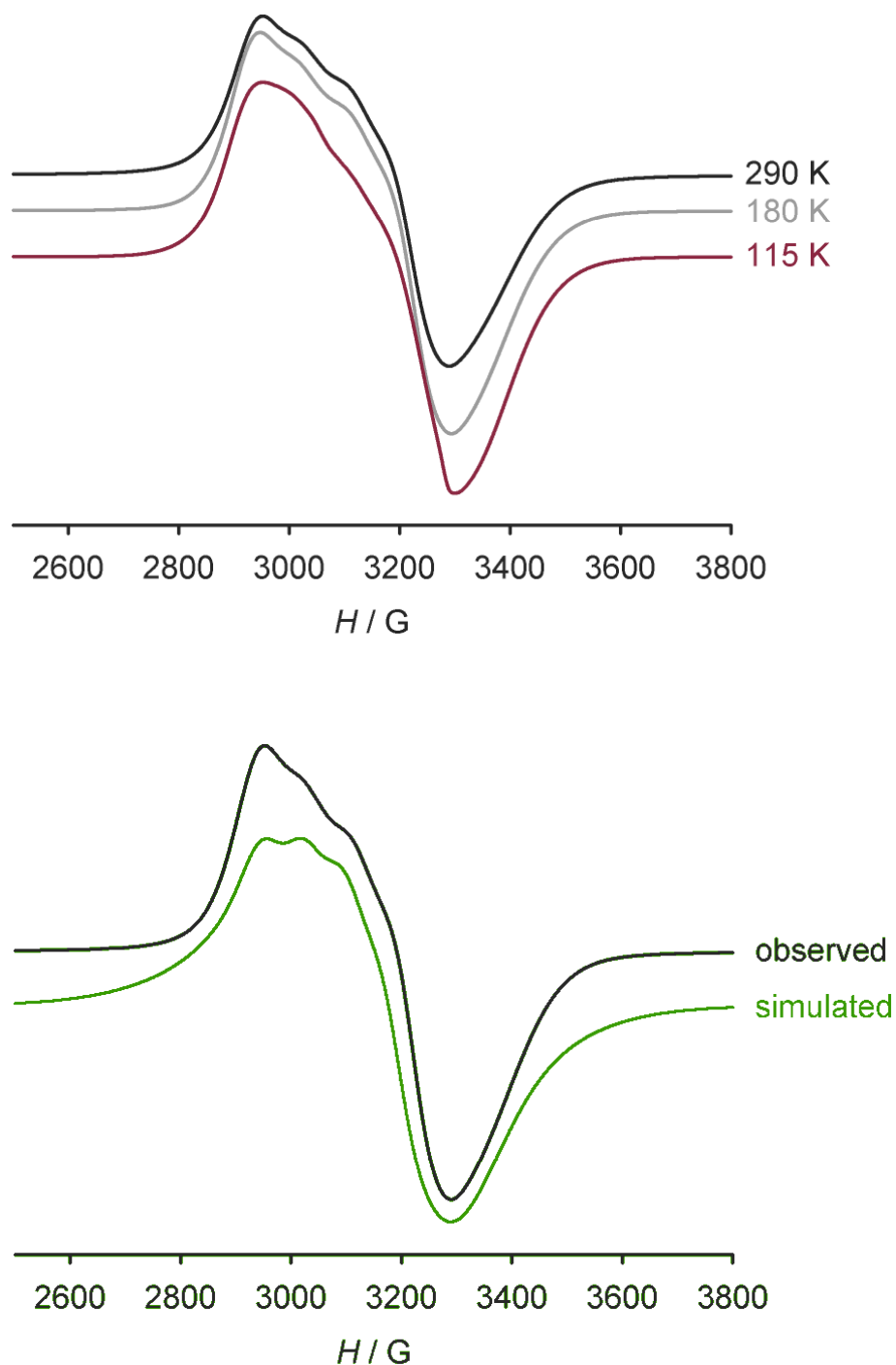
**Figure S2** Top: Powder $X$-band EPR spectra of $[Cu(terpy)_2][BF_4]_2$ at three temperatures. Bottom: Simulation of the spectrum at 290 K.

Parameters: $g_1 = 2.22$, $g_2 = 2.18$, $g_3 = 2.10$, $A_1\{^{63,65}Cu\} = 75$ G.

These powder spectra resemble those of $[Cu(terpy)_2][PF_6]_2$,[11] which is not isostructural with the $BF_4^-$ salt but adopts a closely related structure of the "terpyridine embrace" type.[14] The "inverse" pattern of $g$ values with $g_3 > 2.00$, and $A_1$ half its normal value, are consistent with a $\{d_{y2-z2}\}^1$ configuration at copper, with a disordered axis of elongation.[15] The near-invariance of these spectra with temperature suggests this disorder may be static, rather than dynamic.
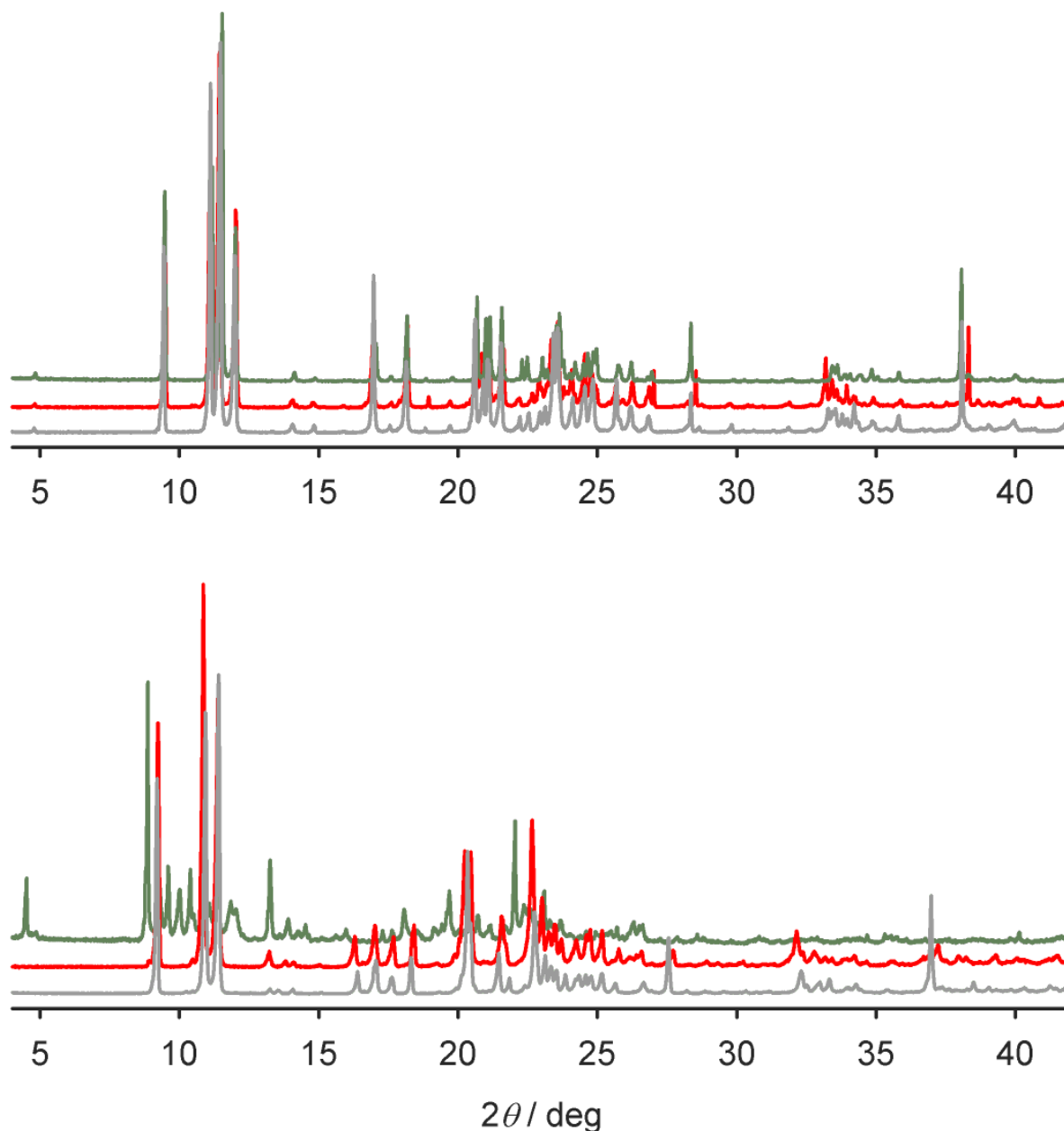
**Figure S3** *X*-ray powder diffraction data for the precursor compounds [M(bpp)$_2$][BF$_4$]$_2$ (top) and [M(terpy)$_2$][BF$_4$]$_2$·$n$H$_2$O (bottom; M$^{2+}$ = Fe$^{2+}$, green; M$^{2+}$ = Cu$^{2+}$, red; M$^{2+}$ = Zn$^{2+}$, gray).

The three [M(bpp)$_2$][BF$_4$]$_2$ solids are isostructural with each other, in agreement with their previously published single crystal structure data.[1-3]

[Cu(terpy)$_2$][BF$_4$]$_2$ and [Zn(terpy)$_2$][BF$_4$]$_2$ are isostructural with each other, but not with [Fe(terpy)$_2$][BF$_4$]$_2$·½H$_2$O.

The more complicated powder pattern for [Fe(terpy)$_2$][BF$_4$]$_2$·½H$_2$O, and the comparison with the data from **3a** (Fig. S13), suggest that it may contain a mixture of two or more crystal phases. Unfortunately, single crystals of this complex suffer from twinning, which prevented a meaningful single crystal structure analysis from being obtained.

**Table S4** Spin-crossover parameters for **1a** and **2a**, from magnetic susceptibility and DSC measurements. DSC data were obtained with a warming temperature ramp, and $\Delta H$ and $\Delta S$ are quoted per mole of iron in the solid solutions.

| Susceptibility | $T_{\frac{1}{2}}\downarrow$ / K | $T_{\frac{1}{2}}\uparrow$ / K | DSC | $T_{\frac{1}{2}}\uparrow$ / K | $\Delta H$ / kJ mol$^{-1}$ | $\Delta S$ / J mol$^{-1}$ K$^{-1}$ |
|---|---|---|---|---|---|---|
| **1a** | 260.0 | 261.6 | | 261.3 | 14.3(3) | 55(1) |
| **2a** | 258.8 | 262.1 | | 261.1 | 16.3(2) | 62.5(8) |
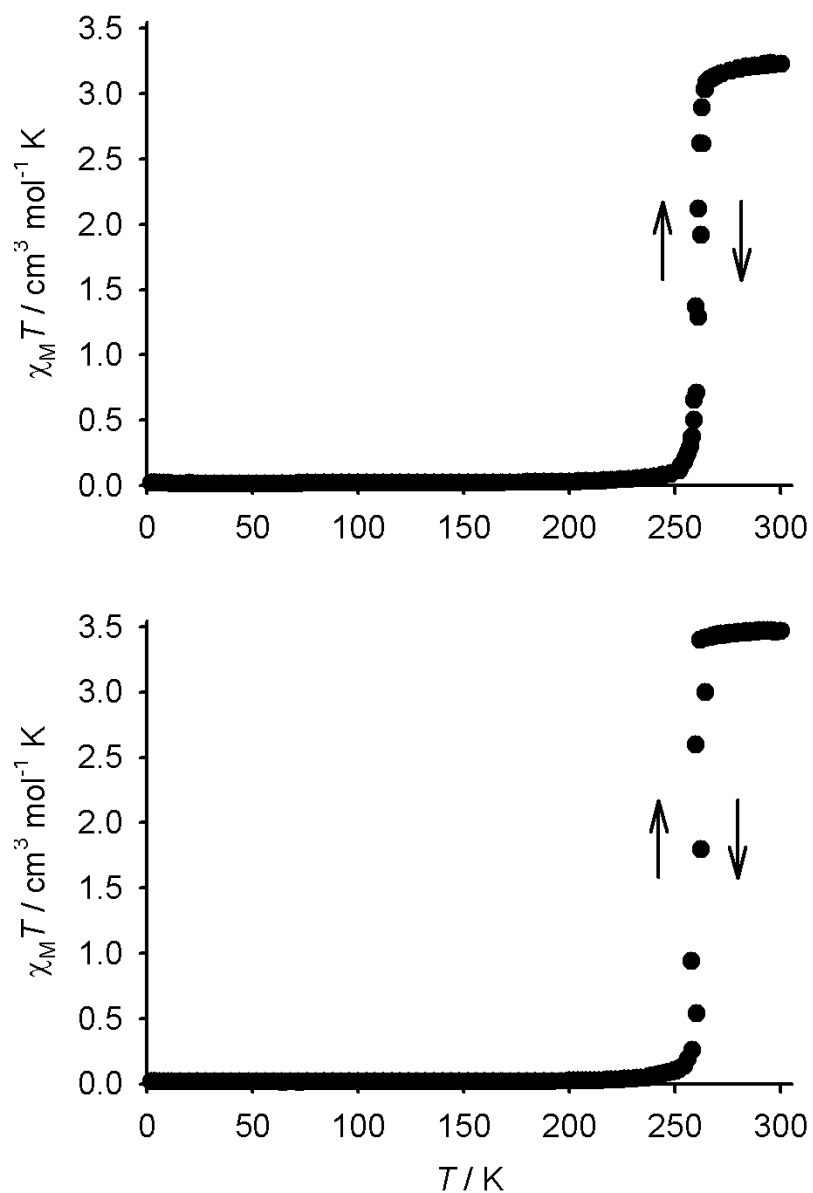


**Figure S4** Magnetic susceptibiliy data for [Cu(terpy)$_2$]$_y$[Fe(bpp)$_2$]$_{1-y}$[BF$_4$]$_2$ (**1a**, top) and [Fe$_y$Cu$_{1-y}$(bpp)$_2$][BF$_4$]$_2$ (**2a**, bottom). Data were measured in cooling and warming mode.
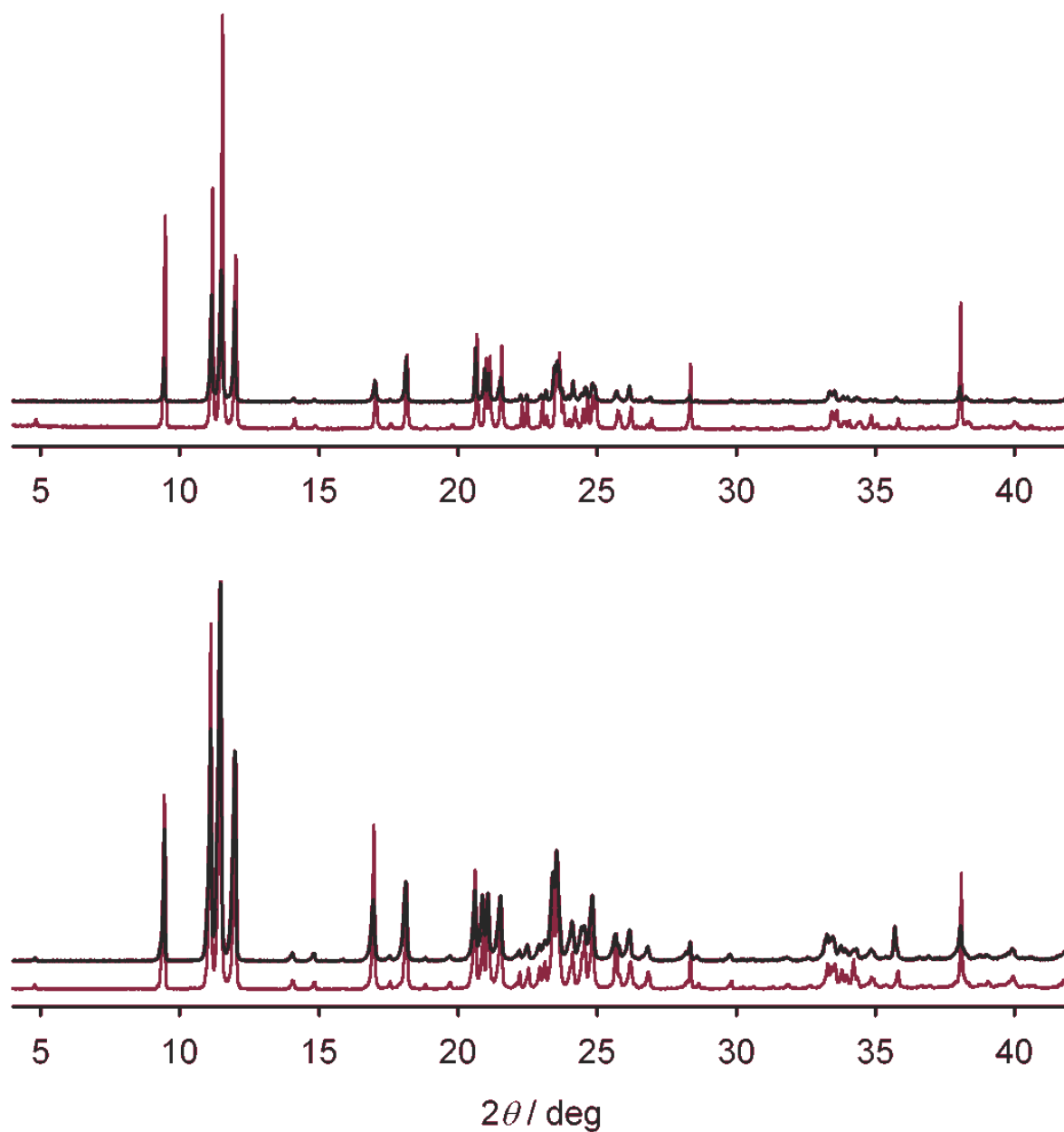
**Figure S5** Black traces: *X*-ray powder diffraction patterns of $[Cu(terpy)_2]_y[M(bpp)_2]_{1-y}[BF_4]_2$ ($M^{2+} = Fe^{2+}$ [**1a**], top; $M^{2+} = Zn^{2+}$ [**1b**], bottom). Maroon traces: powder diffraction data for the corresponding undoped host lattices $[M(bpp)_2][BF_4]_2$ ($M^{2+} = Fe^{2+}$ or $Zn^{2+}$).

The solid solutions **1a** and **1b** are phase-pure, and isostructural with the pure $[M(bpp)_2][BF_4]_2$ host lattices.
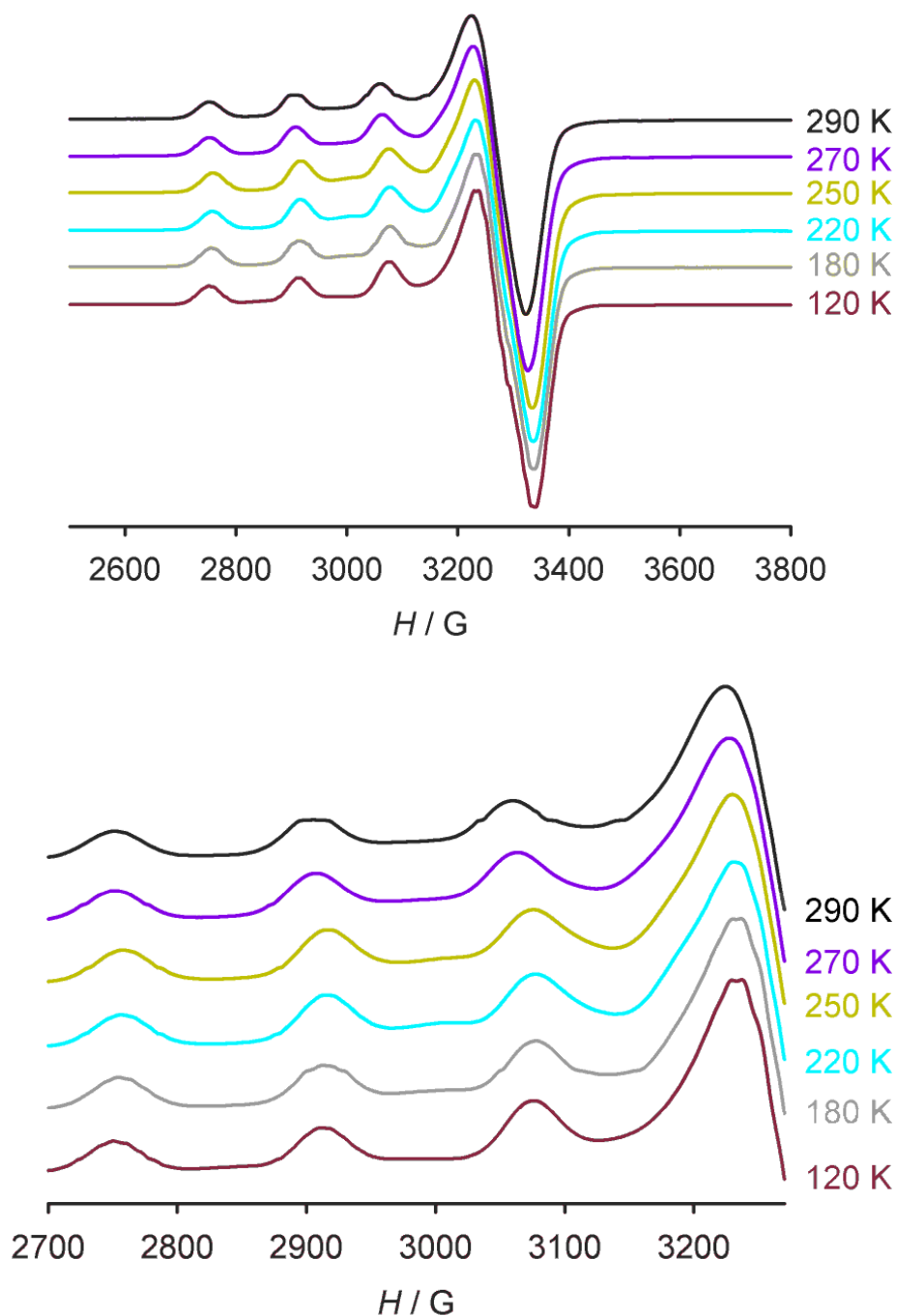
**Figure S6** Top: variable temperature *X*-band EPR spectra of $[Cu(terpy)_2]_y[Fe(bpp)_2]_{1-y}[BF_4]_2$ (**1a**). Bottom: expansion of the parallel region of the spectra.

The spin-state transition in the iron host lattice occurs at 260 K. There appears to be a small decrease in $g_1$ on cooling at $T \leq 250$ K, compared to the higher temperature spectra, that could be attributed to the effects of the spin-transition. There is no significant change in line-width between any of these temperatures, however.

Simulation parameters (see Fig. S8 for a typical simulation):
At 290 and 270 K: $g_1 = 2.29$, $g_2 = 2.10$, $g_3 = 2.07$, $A_1\{^{63,65}Cu\} = 158$ G.
At 250-120 K: $g_1 = 2.28$, $g_2 = 2.10$, $g_3 = 2.06$, $A_1\{^{63,65}Cu\} = 158$ G.
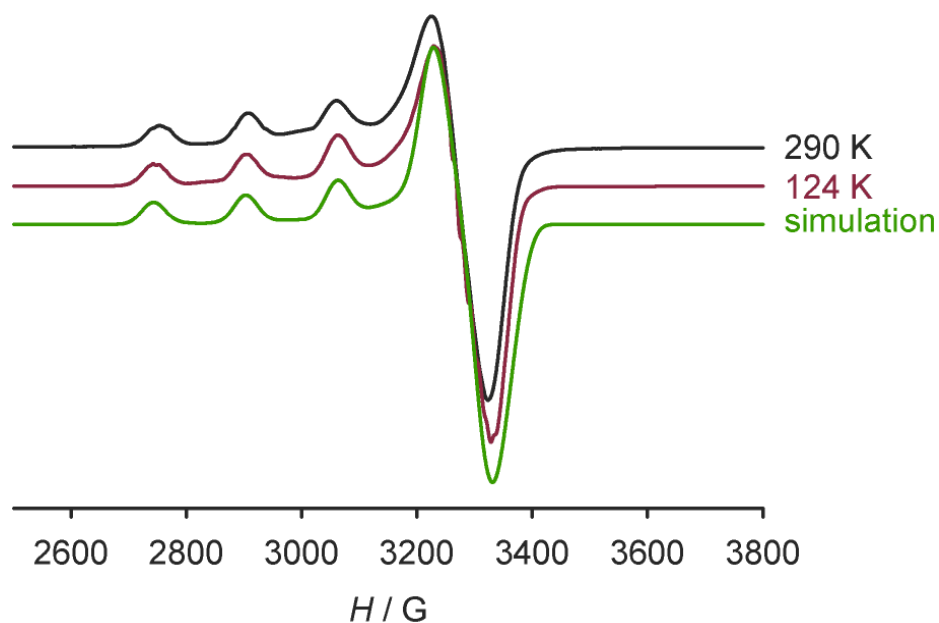
**Figure S7** *X*-band EPR spectra of $[Cu(terpy)_2]_y[Zn(bpp)_2]_{1-y}[BF_4]_2$ (**1b**), and a simulation of the low temperature spectrum.

The spectra are indistinguishable, apart from the partial resolution of $^{14}N$ superhyperfine coupling in the perpendicular feature of the low-temperature spectrum. Notably the small changes at 260 K observed for **1a** are not present in these spectra.

Parameters: $g_1 = 2.29$, $g_2 = 2.10$, $g_3 = 2.06$, $A_1\{^{63,65}Cu\} = 160$ G, $A_{2,3}\{^{14}N\} = 13$ G.
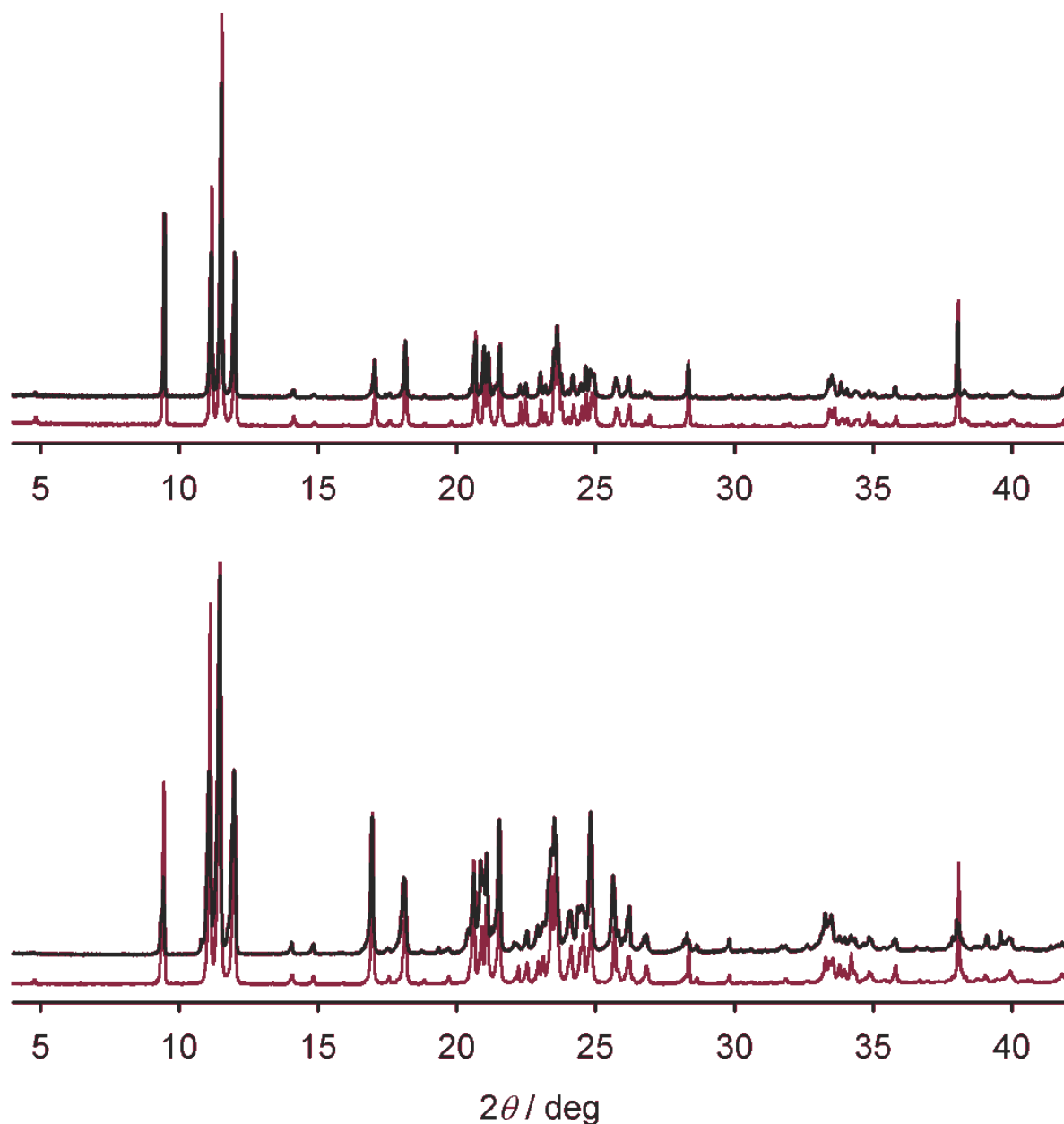
**Figure S8** Black traces: *X*-ray powder diffraction patterns of $[Cu_yM_{1-y}(bpp)_2][BF_4]_2$ ($M^{2+} =$ $Fe^{2+}$ [**2a**], top; $M^{2+} = Zn^{2+}$ [**2b**], bottom). Maroon traces: powder diffraction data for the corresponding undoped host lattices $[M(bpp)_2][BF_4]_2$ ($M^{2+} = Fe^{2+}$ or $Zn^{2+}$).
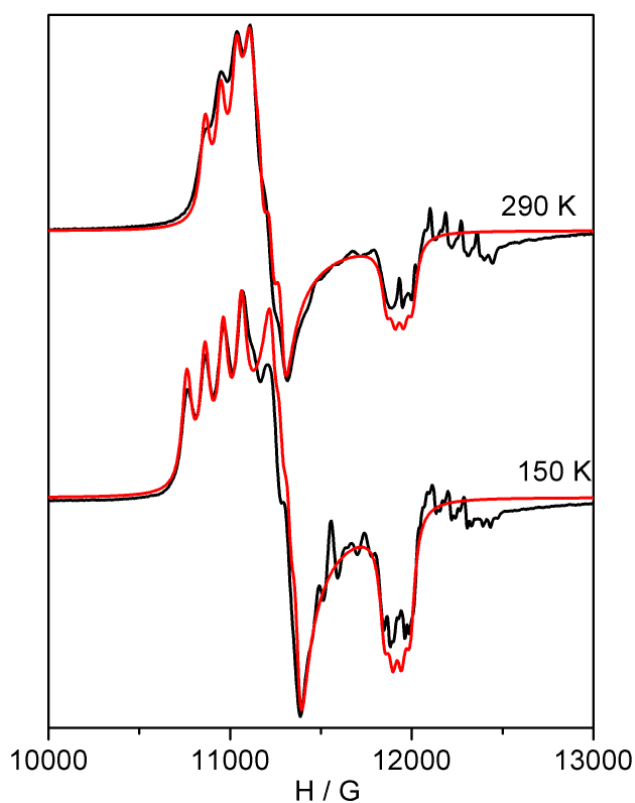
The solid solutions **2a** and **2b** are phase-pure, and isostructural with the pure precursor compounds.
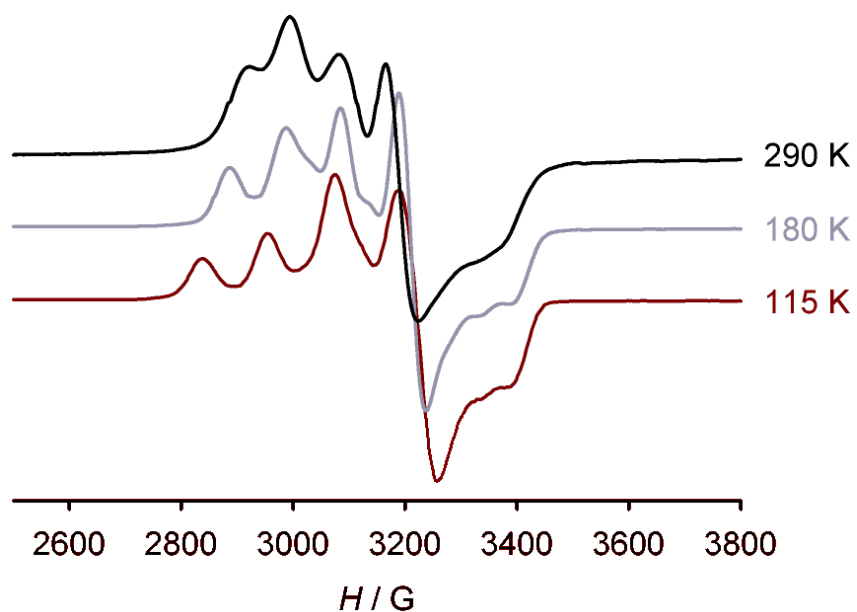
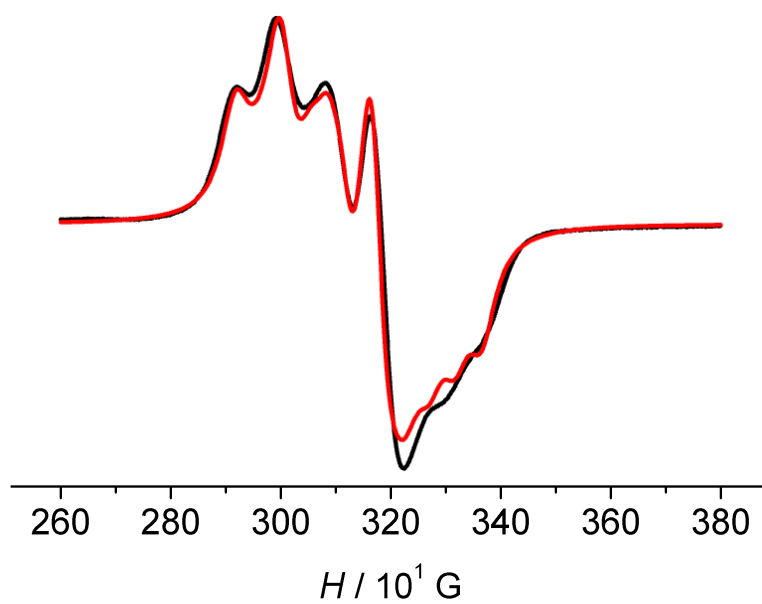**Figure S9** *X*-band EPR spectra of $[Fe_yCu_{1-y}(bpp)_2][BF_4]_2$ (**2a**) at 290 K (black), 180 K (gray) and 115 K (red). The 290 and 115 K spectra are also shown in Fig. 1 of the main paper.
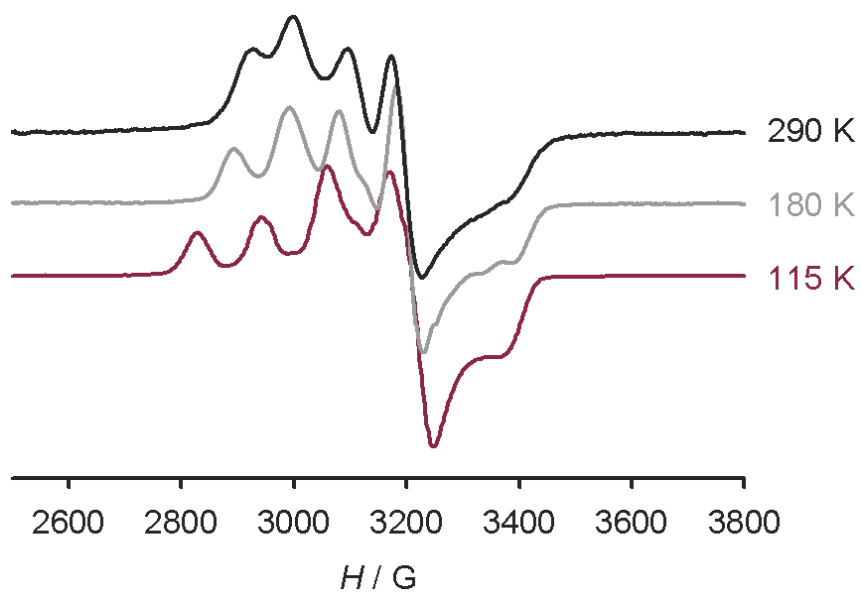


**Figure S10** *X*-band EPR spectra of $[Zn_yCu_{1-y}(bpp)_2][BF_4]_2$ (**2b**) at 290 K (black), 180 K (gray) and 115 K (red).

**Figure S11** Experimental (black) and simulated (red) $Q$-band EPR spectra of $[Fe_yCu_{1-y}(bpp)_2][BF_4]_2$ (**2a**). Comparable data for **2b** are given in the main paper.



**Figure S12** Experimental (black) and simulated (red) $X$-band EPR spectrum of $[Fe_yCu_{1-y}(bpp)_2][BF_4]_2$ (**2a**) at 290 K. The simulation parameters are the same as those used to simulate the $Q$-band spectrum at 150 K (Table 1 of the main paper).
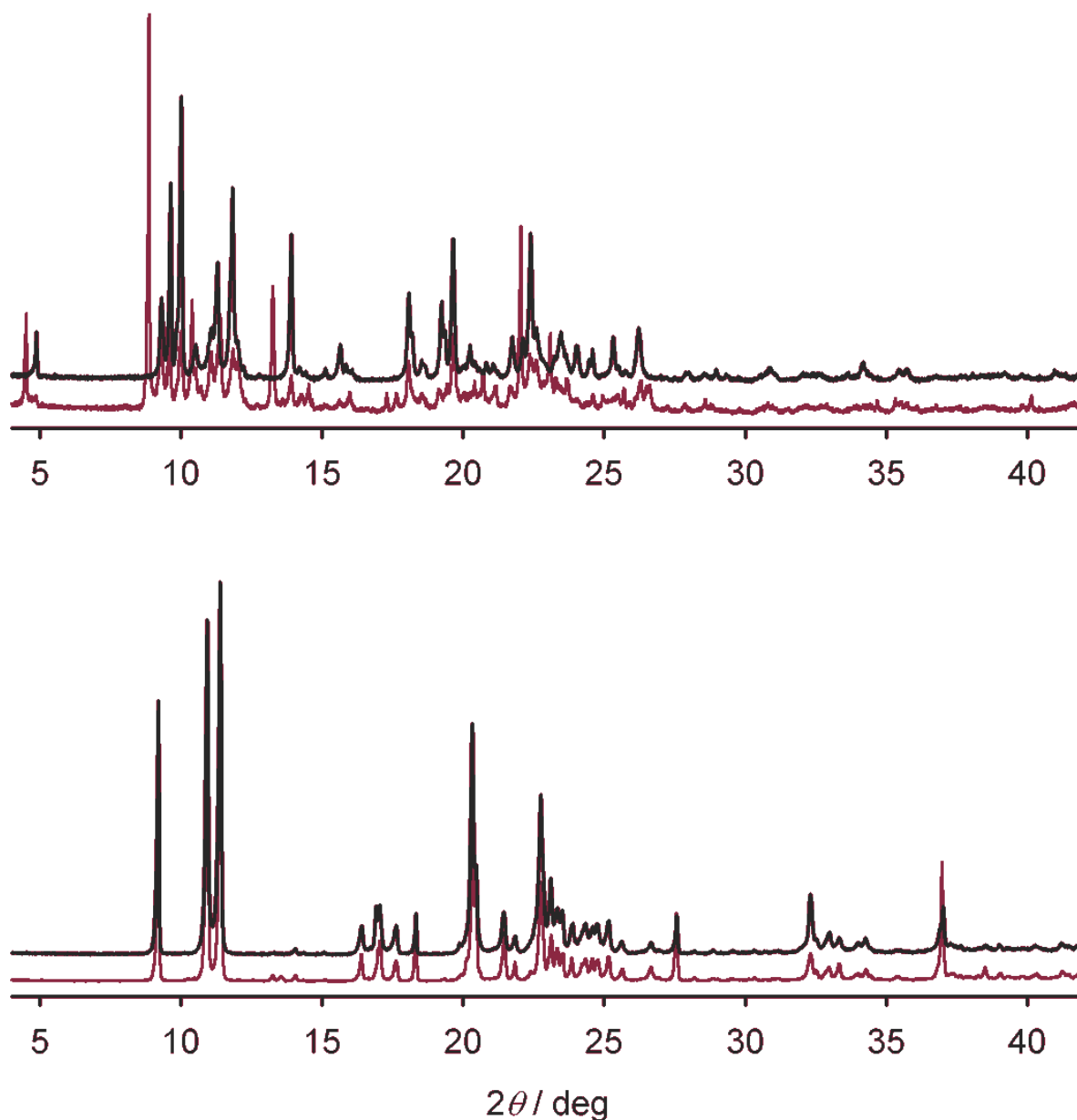
**Figure S13** Black traces: *X*-ray powder diffraction patterns of $[Cu(bpp)_2]_y[Fe(terpy)_2]_{1-y}[BF_4]_2 \cdot \frac{1}{2}H_2O$ (**3a**, top) and $[Cu(bpp)_2]_y[Zn(terpy)_2]_{1-y}[BF_4]_2$ (**3b**, bottom). Maroon traces: powder diffraction data for the corresponding undoped host lattices $[Fe(terpy)_2][BF_4]_2 \cdot \frac{1}{2}H_2O$ and $[Zn(terpy)_2][BF_4]_2$.

The solid solution **3b** is phase-pure, and isostructural with pure $[Zn(terpy)_2][BF_4]_2$. In contrast, the match between the powder patterns of **3a** and $[Fe(terpy)_2][BF_4]_2 \cdot \frac{1}{2}H_2O$ is good, but not perfect.

There is no evidence by EPR for phase separation in **3a** into pure $[Fe(terpy)_2][BF_4]_2 \cdot \frac{1}{2}H_2O$ and $[Cu(bpp)_2][BF_4]_2$ which would, in any case, have only a minor effect on the powder pattern because of the small fraction of the copper complex present. Therefore, we propose that $[Fe(terpy)_2][BF_4]_2 \cdot \frac{1}{2}H_2O$ contains a mixture of two or more solid phases (Fig. S3), and that the distribution of these phases in **3a** is different from the sample of $[Fe(terpy)_2][BF_4]_2 \cdot \frac{1}{2}H_2O$ that was measured.
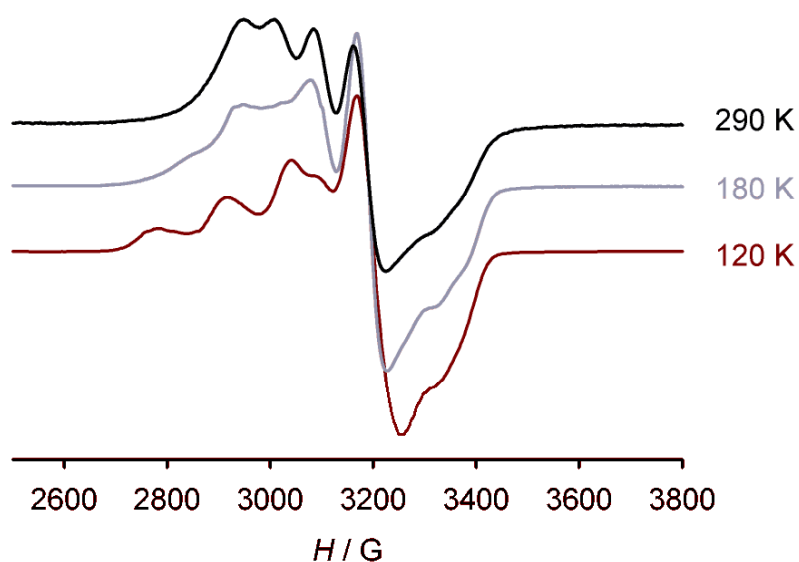
**Figure S14** *X*-band EPR spectra of $[Cu(bpp)_2]_y[Fe(terpy)_2]_{1-y}[BF_4]_2 \cdot \frac{1}{2}H_2O$ (**3a**) at 290 K (black), 180 K (gray) and 120 K (red).

These spectra are broadly similar to those of **2a** and **2b**, but with extra weak features between 3000-3200 G that may imply the presence of more than one copper(II) center in this sample. That was confirmed by the *Q*-band spectra shown on the next page.
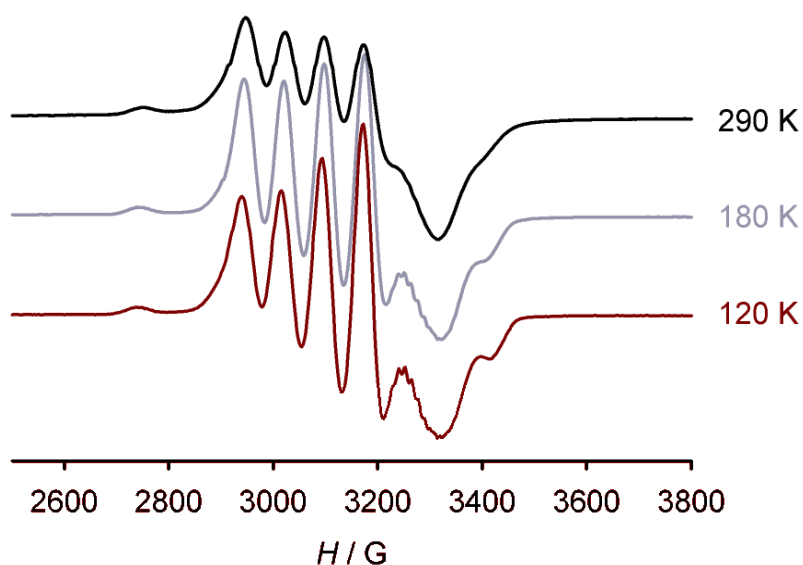


**Figure S15** *X*-band EPR spectra of $[Cu(bpp)_2]_y[Zn(terpy)_2]_{1-y}[BF_4]_2$ (**3b**) at 290 K (black), 180 K (gray) and 120 K (red).

The main parts of these spectra are comparable to **2a**, **2b** and **3a**. They do not vary with temperature, apart from some line-narrowing on cooling. In addition, extra features around 2750 and 3350 G (with visible superhyperfine structure at low T) are not shown by those other solid solutions, and resemble components in the spectra of **1a** and **1b** (Figs. S7 and S8).

We infer from this that **3b** contains a mixture of copper(II) sites including $[Cu(bpp)_2]^{2+}$, and $[Cu(terpy)_2]^{2+}$ and/or other $\{d_{y2-z2}\}^1$ centers such as $[Cu(terpy)(bpp)]^{2+}$.
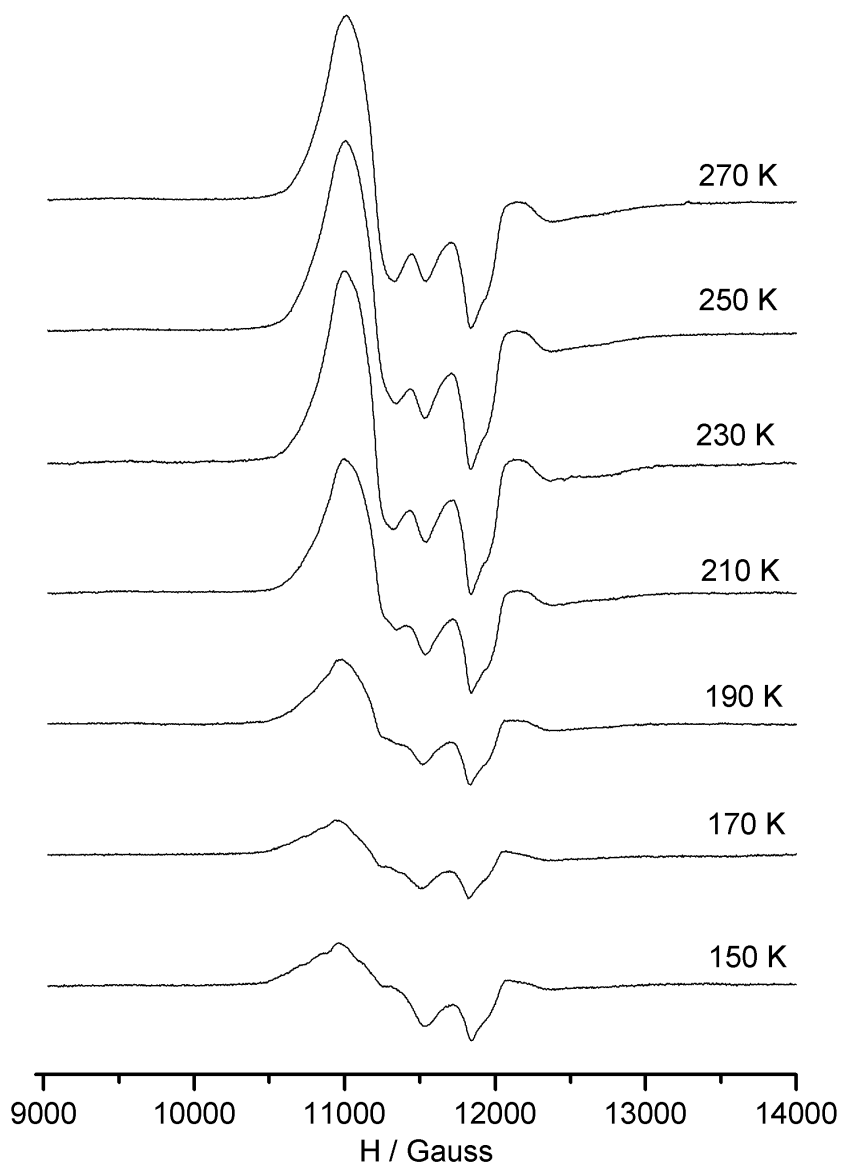
**Figure S16** $Q$-band EPR spectra of $[Cu(bpp)_2]_y[Fe(terpy)_2]_{1-y}[BF_4]_2 \cdot \frac{1}{2}H_2O$ (**3a**).

These spectra show poorer resolution that those of **2a** and **2b** (Fig. 2 of the main paper), and contain an extra feature at 11.5 kG implying the presence of a second copper(II) environment in the material. That is consistent with the $X$-band spectra of this compound (Fig. S14).

This second copper site could result from ligand exchange between the Cu and Fe centers (*c.f.* **3b**, Fig. S13), although this seems less likely given the kinetic inertness of $[Fe(terpy)_2]^{2+}$. Alternatively, it might reflect the existence of more than one crystal phase in the sample (Fig. S13).

In the light of these ambiguities, further characterisation of **3a** and **3b** was not pursued.

# References

1. J. M. Holland, J. A. McAllister, Z. Lu, C. A. Kilner, M. Thornton-Pett and M. A. Halcrow, *Chem. Commun.*, 2001, 577.

2. N. K. Solanki, E. J. L. McInnes, F. E. Mabbs, S. Radojevic, M. McPartlin, N. Feeder, J. E. Davies and M. A. Halcrow, *Angew. Chem.*, *Int. Ed.*, 1998, **37**, 2221.

3. N. K. Solanki, M. A. Leech, E. J. L. McInnes, F. E. Mabbs, J. A. K. Howard, C. A. Kilner, J. M. Rawson and M. A. Halcrow, *J. Chem. Soc., Dalton Trans.*, 2002, 1295.

4. C. J. O'Connor, *Prog. Inorg. Chem.*, 1982, **29**, 203.

5. S. Stoll and A. Schweiger, *J. Magn. Reson.*, 2006, **178**, 42.

6. G. M. Sheldrick, *Acta Cryst., Sect. A*, 2008, **64**, 112.

7. L. J. Barbour, *J. Supramol. Chem.*, 2001, **1**, 189.

8. *POVRAY* v. 3.5, Persistence of Vision Raytracer Pty. Ltd., Williamstown, Victoria, Australia, 2002.

9. A. L. Spek, *J. Appl. Cryst.*, 2003, **36**, 7.

10. (a) W. Henke and D. Reinen, *Z. Anorg. Allg. Chem.*, 1977, **436**, 187;
    (b) R. Allmann, W. Henke and D. Reinen, *Inorg. Chem.*, 1978, **18**, 378.

11. (a) J. V. Folgado, W. Henke, R. Allmann, H. Stratemeier, D. Beltrán-Porter, T. Rojo and D. Reinen, *Inorg. Chem.*, 1990, **29**, 2035;
    (b) W. Bietsch, A. Mirea, T. Kamleiter, M. Weiss, U. S. Schubert, C. H. Weidl, C. Eschbaumer, I. Ovchinnikov and N. Domracheva, *Mol. Phys.*, 2002, **100**, 1957.

12. J. D. Dunitz, V. Schomaker and K. N. Trueblood, *J. Phys. Chem.*, 1988, **92**, 856.

13. (a) B. J. Hathaway, *Struct. Bonding (Berlin)*, 1984, **57**, 55;
    (b) L. R. Falvello, *J. Chem. Soc., Dalton Trans.*, 1997, 4463.

14. M. I. Arriortua, T. Rojo, J. M. Amigo, G. Germain and J. P. Declercq, *Acta Cryst., Sect. B*, 1982, **38**, 1323.

15. (a) B. Hathaway, M. Duggan, A. Murphy, J. Mullane, C. Power, A. Walsh and B. Walsh, *Coord. Chem. Rev.*, 1981, **36**, 267;
    (b) M. A. Halcrow, *Dalton Trans.*, 2003, 4375.